Analysis of in-patient evolution of Escherichia coli reveals potential links to relapse of bone and joint infections

Stanislas Thiriet-Rupert, Jérôme Josse, David Perez-Pascual, Jason Tasse, Camille Andre, Lélia Abad, David Lebeaux, Jean-Marc Ghigo, Frédéric Laurent, Christophe Beloin

Analysis of *in-patient* evolution of *Escherichia coli* reveals potential links to relapse of bone and joint infections

Running title (40 characters): in-patient evolution of *E. coli* in BJIs

Major article

Stanislas THIRIET-RUPERT[1], Jérôme JOSSE[2], David PEREZ-PASCUAL[1$], Jason TASSE[2], Camille ANDRE[2], Lélia ABAD[2], David LEBEAUX[1,3,4], Jean-Marc GHIGO[1], Frédéric LAURENT[2] and Christophe BELOIN*[1]

[1] *Institut Pasteur, Université de Paris-Cité, Genetics of Biofilms Laboratory F- 75015 Paris, France.*

[2] *CIRI, Centre International de Recherche en Infectiologie, Inserm, U1111, Université Claude Bernard Lyon 1, CNRS, UMR5308, École Normale Supérieure de Lyon, 69007, France.*

[3] *Département de Maladies Infectieuses et Tropicales, AP-HP, Hôpital Saint-Louis, Lariboisière, F-75010 Paris, France.*

[4] *FHU PROTHEE*

***Corresponding authors:** Christophe BELOIN, Institut Pasteur, Université de Paris-Cité, Genetics of Biofilms Laboratory F- 75015 Paris, France, christophe.beloin@pasteur.fr (ORCID: 0000-0002-0344-3443)

Author contributions: C.B., S.T.-R., F.L., J.J. designed the experiments. S.T.-R, J.J., D.P.-P, J.T., C.A., and L.A. performed the experiments. C.B., S.T.-R, F.L., J.J., D.L. and J.-M.G. analyzed data. S.T.-R., C.B. and J.J. wrote the manuscript with significant help of D.L., F.L. and J.-M.G.

Abstract: 148 words; Main text: 3476 words

40-word-or-less summary: Here, we identify that three *E. coli* strains involved in bone and joint infection (BJI) relapses adapted in-patient through various molecular mechanisms allowing to outcompete other bacteria or evading immune system. Understanding in-patient adaptation may help fighting relapses in BJIs.

Abstract

Bone and joint infections (BJIs) are difficult to treat and affect a growing number of patients, in which relapses are observed in 10-20% of the case. These relapses, which call for prolonged antibiotic treatment and increase resistance emergence risk, may originate from ill understood adaptation of the pathogen to the host. Here, we investigated three pairs of *Escherichia coli* strains from BJI cases and their relapses to unravel in-patient adaptation. Whole genome comparison presented evidence for positive selection and phenotypic characterization showed that biofilm formation remained unchanged, contrary to what is usually described in such cases. Although virulence was not modified, we identified the loss of two virulence factors contributing to immune system evasion in one of the studied strains. Other strategies, including global growth optimization and colicin production, likely allowed the strains to outcompete competitors. This work highlights the variety of strategies allowing in-patient adaptation in BJIs.

Keywords: BJI, adaptation, relapse, *Escherichia coli*

Background

Bone and joint infections (BJIs), including prosthetic joint infections (PJI), are severe and difficult to treat infections affecting a growing number of patients, and showing 10 to 20% of relapse [1–6]. Although staphylococci are responsible for more than 50% of all BJI, 20% of them are caused by *Enterobacterales*, especially in the case of early and late acute infections [7], whereas *Pseudomonas aeruginosa* infections are associated with particularly difficult to treat BJI [6]. These data therefore support the need to study BJI caused by both Gram-positive and Gram-negative bacteria and for a better understanding of the *in vivo* adaptation leading to relapses.

During host colonization, pathogenic bacteria must face the endogenous microbiota or other co-infecting bacteria. This competition could involve toxin production [8,9] and other adaptive strategies to access resources [10] and evade the host immune system [11,12], eventually leading to a decrease virulence accounting for bacterial persistence in the host.

The genetic modifications underlying these adaptations are in general quite restricted upon natural host purifying selection [13,14]. In some extreme cases, mutator genotypes can evolve, thus facilitating within-host adaptation [15,16]. Extensive genome reductions and rearrangements [17–19] are also observed leading to the loss of non-essential genes in the host environment. However, there is an increasing body of evidence that these gene losses could also fuel adaptative evolution and microbial adaptation within patient is currently under intense scrutiny [20,21]. However, acquiring longitudinal samples and studying pathogens adaptation from the same patient in the context of infection relapses is difficult [22]. In this study, we analysed three pairs of *E. coli* strains isolated from initial and recurrent BJIs in 3 patients to

investigate how in-patient evolution occurred in these situations and provide insights on the potential mechanisms involved in infection relapse.

Methods

Selection of clinical strains

Initial/Relapse pairs of clinical *E. coli* strains used in this study were selected among the routine collections of the Bacteriology Department of Hôpital de la Croix-Rousse, Hospices Civils de Lyon and the Bacteriology laboratory at Cerballiance, Lyon. The first search criterion corresponded to collect *E. coli* strains isolated from BJI from 2017 to 2020. Then, initial/relapse pairs were formed when *E. coli* strain was isolated in two different samples at two different times in the same patient (initial and relapse) and at the same site of infection. Strain characteristics are available in Table 1. Antimicrobial susceptibility tests were performed by using the disc diffusion method (Supplementary Table 1).

Bacterial strains and growth conditions

Bacterial strains used in this study are listed in Supplementary Table 2. Bacteria were grown in Miller's Lysogeny Broth (LB) (Corning) or M63B1 minimum medium supplemented with appropriate antibiotic and carbon source as specified. Liquid cultures were incubated at 37°C or 30°C with 180rpm shaking. Solid cultures were done on LB with 1.5% agar supplemented with the appropriate antibiotics. Chemicals and media were purchased from Sigma-Aldrich.

Strain construction

Insertion of a Zeo-GFP and Zeo-mars genetic cassettes at the permissive lambda *att* attachment site as well as the deletion of *fliC* in I1 and R1 strains and the deletion of two adhesin coding genes in I2 strain were done using pKOBApra plasmid [23] and lambda-red recombination. Primers used for genetic constructions are listed in Supplementary Table 3.

CFU counting on biomaterials

The biofilm forming capacity was assessed on different orthopaedic biomaterials [stainless steel (AISI 316L), titanium (TA6V), medical grade silicone and ultra-high molecular weight polyethylene (UHMWPE)]. Uniform cylindrical pegs of orthopaedic biomaterial were manufactured by a supplier of medical and surgical orthopaedics equipment (Groupe Lépine, Genay, France) under the same conditions of manufacture of orthopaedic biomaterial and sterilised by gamma rays. Biomaterial pegs were fixed into the lid of 24-well flat bottom cell culture plates (Corning Inc., Corning, NY, USA). Bacterial biofilms were formed by immersing the lid-containing pegs into 2mL of cultures at OD_{600}=0.05 and incubated in LB for 24 hours at 37°C in humid atmosphere. After 3 rinsing steps in PBS, the pegs were dropped in a Falcon tube containing 5mL of PBS for biofilm disruption using sonication for 5 minutes (BACTOSONIC 14.2, BANDELIN, Berlin, Germany). Then, viable cell count was determined by serial dilution and plating.

Bacterial adhesion to MG63 human osteoblastic cells

The osteoblastic cell line MG63 (LGC standards, Molsheim, France) was used to test bacterial adhesion. Cells were cultured in 75cm² flasks (T75, BD Falcon, Le Pont de Claix, France) at 37°C under 5% CO_2, in a culture medium composed of DMEM (Dulbecco's Modified Eagle Medium containing D-glucose, L-glutamine, pyruvate) supplemented with 10% fetal calf serum (FCS), penicillin (100µg/mL) and streptomycin (100µg/mL), all from Gibco (Paisley, UK).

Cells were passaged once a week and used until passage 25 at the most. The day before the infection, MG63 cells were seeded at 100,000 cells per well in a 24-well plate and the different bacterial strains were inoculated in LB. The day of the infection, overnight bacterial cultures were centrifugated, resuspended and adjusted in DMEM + 10% FCS to reach a MOI (multiplicity of infection) of 100:1 and added to cell culture. After 2 hours of infection, cells were washed twice with PBS and incubated and lysed by osmotic shock in sterile water and lysates were plated on tryptone soy agar plates (Biomérieux) using the Easy Spiral® automaton (Interscience, Saint-Nom-la-Bretèche, France). CFU were counted after 18 hours of incubation at 37°C and results were presented as CFU for 100 000 cells.

Survival to human serum

For each strain, 50µL at OD_{600}=0.4 was mixed in a well of a 96-well plate with 50µL of active human serum. The same process was followed for a control with heat inactivated serum (HIS) (30 minutes at 55°C). Plate was then incubated at 37°C under shaking (450rpm) for 1h30. Each well was then serially diluted and plated on LB for CFU count and the survival of each strain was expressed as the ratio between the CFUs in active serum divided by the CFUs in HIS.

Zebrafish infection

Overnight bacterial cultures were centrifuged, washed, and resuspended at the desired concentration in PBS. Anesthetized zebrafish larvae were microinjected intravenously 52–58 hours post-fertilization with 1nL of each bacterial suspension at a final concentration of $2x10^3$ CFU [24]. Infected larvae were transferred into individual wells containing 1mL of Volvic water (Danone, France) and 0.003% 1-phenyl 2-thiourea (used to improve optical transparency in zebrafish) in 24-well plates, incubated at 28°C, and regularly observed under a

144 stereomicroscope. Protocols describing zebrafish maintenance and analysis, see the
145 corresponding supplementary method section.
146
147 **Competition assay for biofilm formation**
148 The pair of strains used in competition assay carried two different fluorescent tags and were
149 inoculated in LB medium supplemented with appropriate antibiotic and incubated overnight at
150 37°C under shaking. Cultures were then adjusted to OD_{600} = 0.05 and mixed in 1:1 ratio
151 (verified by FACS). Each competition mix was then inoculated in a PVC plate and incubated
152 at 37°C for 16 hours. The supernatant was removed from each well, the biofilm resuspended in
153 100µL of PBS and the proportion of each strain was assessed by FACS and the relative fitness
154 calculated as follows:

155 $$relative\ fitness = \frac{\left(\frac{Target_{post}}{Target_{pre}}\right)}{\left(\frac{ref_{post}}{ref_{pre}}\right)}$$

156 , where $Target_{pre}$ and $Target_{post}$ are the cell concentrations of the target strain in the mixed
157 culture before and after the overnight incubation, and ref_{pre} and ref_{post} are the cell concentrations
158 of the corresponding reference strain. In order to account for growth differences due to the
159 expression of one or the other fluorescent tag (supplementary Figure 1), competitions were run
160 with both possible combinations of fluorescent tags. This protocol was used to compete R1 and
161 R3 strains against their respective ancestors. However, because GFP and RFP tags were not
162 expressed in I2 and R2 strains, we used an alternative strategy based on PCR amplification and
163 Sanger sequencing of a SNP locus allowing to destinguich both strains (see supplementary
164 method section).
165
166 **Competition assay for growth in liquid cultures**

The strains were incubated at 37°C in the appropriate medium and adjusted to OD_{600}=0.05. A 1:1 ratio mixed culture was verified by FACS and incubated overnight at 37°C with shaking. The concentrations of target and reference strains was measured using FACS and relative fitness were calculated as above.

SNP analysis

Mutations in the adapted strain were identified by using the genome assembly of its ancestral strain (see supplementary methods) as a reference. breseq version 0.35.0 [25] with the consensus mode was used with default parameters. As a confirmation of this analysis, Freebayes version 1.3.3 [26] was also used to identify SNPs using the following stringent thresholds: minimum depth of 20 reads, a maximum depth corresponding to the average depth over the genome plus one standard deviation, at lease 10 forward and 10 reverse reads supporting the SNP, minimum variant quality of 30, minimum base quality of 20. Only variants identified in both analyses were validated. The resulting identified mutations were filtered out if they were too close to each other (less than 50bp). These mutations are usually the result of misaligned reads, often due to repetitive regions [27]. Because these regions are not 100% identical, they are disturbing the mapping process resulting in false positives. Mutations found in mobile elements were kept if only one copy was present in the genome.

Statistical analysis

Figures and statistical tests were performed using either Prism 9.5.1 for Mac OS X (GraphPad Software, Inc.) or Rstudio with R version 4.2.1 using the R package GGplot2 [28].

Methods related to the supplementary results are available in supplementary methods.

RESULTS

I- In-patient evolved *Escherichia coli* clones showed no antibiotic resistance acquisition but signs of natural selection.

In order to investigate potential cases of in-patient adaptation, we obtained three pairs of *E. coli* strains sampled in three patients presenting relapsing BJIs. Each pair is composed of a sample at the time of the initial infection (strains hereafter denominated as I1 to I3 for cases 1 to 3) and a second sample corresponding to the relapse of this infection (strains hereafter denominated as R1 to R3 for cases 1 to 3). The genome of each strain was sequenced and analyzed to confirm that the infection and relapse strains were indeed the same and not a case of re-infection (Table 1, see supplementary methods). Interestingly, antimicrobial susceptibility testing (supplementary Table 1) and in silico analysis (supplementary Data 1) did not reveal any acquisition of antibiotic resistance associated with the relapse events. Consequently, each strain pair was examined for other phenotypic and genetic features that could have been selected for to allow the infection relapses.

The first notable difference identified by genomic analysis was the number of gained and lost genes (supplementary Table 4), some of which corresponding to potential plasmids (supplementary Data 2, see supplementary methods). Particularly, the R2 strain that displayed the longest in-patient evolution underwent an important genome reduction with the loss of 3.4% of its size corresponding to 170 coding sequences involved in various functions such as transport, iron acquisition, carbohydrate acquisition and utilization, defense against competitors with Microcin H47 production-related genes and three adhesins (supplementary Data 2).

The number of mutation per base per year was quite high for all three relapse strains (1.11×10^{-6} to 8.38×10^{-6}) as compared to what was reported in the literature (6.9×10^{-7} for *E. coli* ED1a in

the gut, [27]). In addition, even if no functional convergence was observed in the mutated genes, the predominance of loss of function and non-synonymous mutations suggests that positive selection was at play in these cases (Table 2, see supplementary methods).

II- *In vivo* adaptation did not modify biofilm formation capacities.

Because strain motility could impact the virulence and biofilm forming capacity, we tested each strain on low-agar LB plates at 30°C and 37°C, which showed that the second and third pairs of strains were non-motile (supplemental Figure 2, see supplementary methods). Both I1 and R1 strains display temperature dependent motility very likely due to a flagellin production restricted to 30°C (supplementary Figure 2 and 3, see Supplementary Results).

Biofilm formation was assessed on various surfaces showing that the R1 relapse strain formed 1.71 more biofilms than I1 strain when grown on silicon coupons (Figure 1.A). No difference was identified for the I2-R2 pair (Figure 1.B), while the I3 strain showed a 1.49 increase in biofilm formation on silicon (Figure 1.C). However, in all cases the tested clinical strains showed a weak biofilm forming capacity, all of them being equivalently or even less efficient than *E. coli* K12 strain MG1655 used as control for weak biofilm formation. Interestingly, R1 strain showed a slight decrease of its adhesion capacity to osteoblasts (Figure 1.D). However, no evident genetic modification could be linked to this phenotype. No difference was observed either in term of auto-aggregation or production of curli amyloids and cellulose (supplementary Figure 4, see supplementary methods and Supplementary Results). Taken together, these results show that very limited differences in biofilm formation were detected within each pair suggesting that a modification of biofilm formation and biofilm-related phenotypes was unlikely to be involved in in vivo adaptation in these three studied cases.

III- Loss of adhesins induces serum resistance in R2 strain.

To assess the strain capacity to challenge to the host immune defenses, we measured the survival of all strains to exposure to active human serum. While we observed no difference between I3 and R3 strains, the relapse strain R1 had a slight decrease in serum resistance compared to I1 strain and the relapse strain R2 had a clear increase in serum resistance relatively to its ancestral strain I2 (Figure 2.A). Although we identified no difference in the I2 vs R2 lipopolysaccharide profile (outer-membrane component targeted by the complement) (Figure 2.B), the loss of two adhesins in R2 could be linked to this phenotype (supplementary Data 2) [11]. Indeed, deletion of each adhesin in I2 strain led to reduced serum resistance suggesting that the loss of both adhesins could have been selected through the conferred immune system evasion, contributing to the strain adaptation to the host environment (Figure 2.C). Unfortunately, we were unable to assess the additive effect of these mutations since we could not reconstruct the double mutant in the I2 strain despite repeated attempts.

IV-Strain virulence was not targeted during in-patient selection.

To gain insight into the potential evolution of the virulence of the studied strains, we assessed their cytotoxicity on HeLa cells as well as hemolysis capacities and showed no differences, except for a slightly lower hemolysis induced by R2 strain after 24h of incubation in presence of defibrinated horse blood (Figure 3.A.B).

Potential differences in in vivo virulence were tested in a zebrafish (*Danio rerio*) larval model [29]. While no differences were found in bacterial load for all pairs (Sup Figure S5.A.B.C), zebrafish larvae exposed to R2 relapse strain had a slightly lower survival, although non-significant, 24 hours post infection (hpi) than with its related ancestor I2, even though both

strains ultimately induced the same level of mortality 48 hpi (Figure 3.C.D). No difference was identified concerning the zebrafish innate immune response level (Figure 3.E). These results suggest that the R2 relapse strain induced a slightly quicker mortality, which does not seem to be linked to a difference in colonization ability.

V- Growth optimization and colicin production as strategies to outcompete other bacteria.

To assess if a difference in growth capacity could advantage the strains isolated after relapses, they were pitted against their related ancestor in 1:1 ratio competition experiments in biofilm and liquid conditions. First, no difference in fitness was observed in biofilm condition, which further straightened the hypothesis that biofilm formation was not targeted during the in vivo adaptation. In liquid, while R1 strain slightly outcompeted its ancestor I1, R2 strain had a striking fitness advantage over I2 (Figure 4.A).

To further investigate this phenotype, we competed I2 and R2 strains in presence of different sugars as well as of an iron chelator (2,2'-Bipyridyl) based on identified genetic modifications and especially gene losses related to uptake and metabolism of these substrates (supplementary Data 2). Surprisingly, despite these gene losses, R2 strain showed no growth defect and even globally had an advantage through a capacity to better sustain growth during stationary phase (supplementary Figure 6), as confirmed by competition assays (Figure 4.B). Therefore, extensive gene loss seems to have resulted in a global growth optimization, which could have helped the strain to outcompete other bacteria including its ancestor.

Another strategy to outcompete its kin and promote subsequent adaptation was identified in the relapse strain R1, which acquired a colicin-producing plasmid allowing the production of colicin E1. An overlay assay indeed confirmed the acquired capacity of R1 relapse strain to inhibit I1 strain growth (supplementary Figure 7).

Discussion

Treatment failure is a common issue of BJIs, allowing bacteria to remain and adapt to the host, ultimately increasing the risks of relapse and the difficulty to cure the patient. A better understanding of the mechanisms underlying pathogens adaptation to the host environment would allow improving the management of relapsing BJIs. Here we investigated three cases of BJIs relapse involving pathogenic *E. coli*.

Our genetic and phenotypic analysis revealed diverse functions arising from bacterial adaptation to the host environment during BJIs. We found that adapted strains isolated from relapses displayed a relatively high mutation rate, which is a_known adaptive advantage increasing the advantageous mutation probability that could be subsequently selected [13,30,31]. However, no mutations were found in genes associated with DNA damage repair, suggesting that these high mutation rates were intrinsic to these strains and could have further promoted the selection of beneficial mutations, partly explaining their adaptive success.

Although biofilms are known to be frequently involved in infections and relapses, none of the three investigated cases showed an increased biofilm formation capacity that could have played a role in the relapses and all strains were even characterized as poor in vitro biofilm formers. While a strong *in vitro* biofilm formation is often linked to the severity of clinical outcomes in prosthesis-related infections [32–34], it did not seem to be a critical factor in this study.

The host immune system exerts a critical selection pressure on pathogenic bacteria. In I1 and R1 strains, the inhibition of flagellin production at 37°C could minimize their recognition by the host's immune defenses [35,36]. This could not only contribute to immune system evasion but also to save energy through a down-regulation or suppression of flagellin production, as shown to be the case in the context of gut infection by *E. coli* [37,38].

This immune system evasion strategy is even clearer in the case of the R2 relapse strain, which showed increased survival to human serum through the loss of two adhesins. This suggests that in these cases, evading the host's immune system may be more critical than maintaining virulence as shown to happen during in vivo adaptation [39,40]. This could allow pathogens to stay longer in the host as shown in the infection experiments performed in zebrafish, where no difference was observed.

In addition, the R2 strain presented an interesting case of gene loss. Genome reduction is usually considered as a strategy selected because energy consumption is reduced via the loss of genes that are not used or under selective pressure [41,42]. In the case of the R2 strain, numerous gene losses seem to result in a global growth capacities optimization, potentially associated to lower the cost for gene production and lower amount of DNA to replicate. It is possible that some nutritional resources could be directly acquired from the new host environment instead of being synthesized by the cells and that the loss of genes involved in this production optimizes the cell metabolism [43]. Gain of growth capacity in the context of an infection could be of paramount importance to outcompete other endogenous or pathogenic bacteria and thrive in the host environment.

The polymicrobial context of some of these BJIs is also an important parameter to stress since the interactions between the different bacterial species or strains could play an important role in the relapses and the mechanisms shaping bacterial adaptation to the host environment [44,45]. This study may therefore have missed some adaptation that rely on bacteria-bacteria direct or indirect interactions. In addition, as for any longitudinal study, there is always a possibility that the strains causing the very initial infection already evolved at the time of sampling when infection was clinically detected, and some of these mutations, that would be undetected in our study, could potentially contribute to the success of the relapse strains.

Finally, the small number of strains studied, and the diversity of BJI cases, make it challenging to draw definitive conclusions about typical strain profiles and mechanisms involved in in vivo adaptation. However, it seems that a higher mutation rate allowing a better adaptability as well as evolving immune system evasion and outcompeting other bacteria are relevant strategies selected in patient. Further investigations with a larger cohort would help determine whether these diverse adaptive strategies constitute a more general rule of *E. coli* pathogenic strain in BJIs.

DATA AVAILABILITY

All sequencing reads as well as genome assembly for each strain were deposited in NCBI under the BioProject accession number PRJNA932763. The code used in this study is available at https://github.com/Sthiriet-rupert/BJIs_adaptation.

COMPETING FINANCIAL INTERESTS

The authors declare no competing financial interests.

ACKNOWLEDGEMENTS.

We thank Dr. Emma Colucci-Guyon and Laurent Boucontet for critical reading of the manuscript. We are grateful to the Zebrafish Projects Hub of the Institut Pasteur and especially to Dr. Emma Colucci-Guyon and Laurent Boucontet who carried out the infection experiments in zebrafish larvae. We are grateful to Dr. Monica Rolando for kindly providing the anti-flagellin antiserum. We are grateful to Emmanuel Chanard from Cerballiance for providing strains and microbiological information.

ETICS STATEMENT

Animal experiments were performed according to European Union guidelines for handling of laboratory animals (http://ec.europa.eu/environment/chemicals/lab_animals/home_en.htm) and were approved by the Institut Pasteur Animal Care and Use Committee and the French Ministry of Research (APAFIS#31827).

FUNDINGS

This work was supported by the French National Research Agency (ANR), project EvolTolAB (ANR-18-CE13-0010), by the French government's Investissement d'Avenir Program, Laboratoire d'Excellence "Integrative Biology of Emerging Infectious Diseases" (grant n°ANR-10-LABX-62-IBEID) and by the Fondation pour la Recherche Médicale (grant DEQ20180339185). S.T.-R was supported by the French National Research Agency (ANR), project EvolTolAB (ANR-18-CE13-0010).

References

1. Osmon DR, Berbari EF, Berendt AR, et al. Diagnosis and management of prosthetic joint infection: clinical practice guidelines by the Infectious Diseases Society of America. Clin Infect Dis. **2013**; 56(1):e1–e25.
2. Tande AJ, Patel R. Prosthetic joint infection. Clin Microbiol Rev. **2014**; 27(2):302–345.
3. Tong SYC, Davis JS, Eichenberger E, Holland TL, Fowler VG. Staphylococcus aureus infections: epidemiology, pathophysiology, clinical manifestations, and management. Clin Microbiol Rev. **2015**; 28(3):603–661.
4. Laurent E, Gras G, Druon J, et al. Key features of bone and joint infections following the implementation of reference centers in France. Med Mal Infect. **2018**; 48(4):256–262.
5. Ferguson J, Alexander M, Bruce S, O'Connell M, Beecroft S, McNally M. A retrospective cohort study comparing clinical outcomes and healthcare resource utilisation in patients undergoing surgery for osteomyelitis in England: a case for reorganising orthopaedic infection services. J Bone Jt Infect. **2021**; 6(5):151–163.
6. Cerioli M, Batailler C, Conrad A, et al. Pseudomonas aeruginosa Implant-Associated Bone and Joint Infections: Experience in a Regional Reference Center in France. Front Med (Lausanne). **2020**; 7:513242.
7. Triffault-Fillit C, Ferry T, Laurent F, et al. Microbiologic epidemiology depending on time to occurrence of prosthetic joint infection: a prospective cohort study. Clin Microbiol Infect. **2019**; 25(3):353–358.

8. Joo H-S, Cheung GYC, Otto M. Antimicrobial activity of community-associated methicillin-resistant Staphylococcus aureus is caused by phenol-soluble modulin derivatives. J Biol Chem. **2011**; 286(11):8933–8940.
9. Majeed H, Gillor O, Kerr B, Riley MA. Competitive interactions in Escherichia coli populations: the role of bacteriocins. ISME J. **2011**; 5(1):71–81.
10. Baishya J, Wakeman CA. Selective pressures during chronic infection drive microbial competition and cooperation. npj Biofilms Microbiomes. Nature Publishing Group; **2019**; 5(1):1–9.
11. Klemm P, Roos V, Ulett GC, Svanborg C, Schembri MA. Molecular characterization of the Escherichia coli asymptomatic bacteriuria strain 83972: the taming of a pathogen. Infect Immun. **2006**; 74(1):781–785.
12. Price EP, Sarovich DS, Mayo M, et al. Within-host evolution of Burkholderia pseudomallei over a twelve-year chronic carriage infection. mBio. **2013**; 4(4):e00388-13.
13. Lieberman TD, Flett KB, Yelin I, et al. Genetic variation of a bacterial pathogen within individuals with cystic fibrosis provides a record of selective pressures. Nat Genet. **2014**; 46(1):82–87.
14. Marvig RL, Johansen HK, Molin S, Jelsbak L. Genome analysis of a transmissible lineage of pseudomonas aeruginosa reveals pathoadaptive mutations and distinct evolutionary paths of hypermutators. PLoS Genet. **2013**; 9(9):e1003741.
15. Klemm EJ, Gkrania-Klotsas E, Hadfield J, et al. Emergence of host-adapted Salmonella Enteritidis through rapid evolution in an immunocompromised host. Nat Microbiol. Nature Publishing Group; **2016**; 1(3):1–6.
16. Feliziani S, Marvig RL, Luján AM, et al. Coexistence and Within-Host Evolution of Diversified Lineages of Hypermutable Pseudomonas aeruginosa in Long-term Cystic Fibrosis Infections. PLoS Genet. **2014**; 10(10):e1004651.
17. Smith EE, Buckley DG, Wu Z, et al. Genetic adaptation by Pseudomonas aeruginosa to the airways of cystic fibrosis patients. Proc Natl Acad Sci U S A. **2006**; 103(22):8487–8492.
18. Losada L, Ronning CM, DeShazer D, et al. Continuing evolution of Burkholderia mallei through genome reduction and large-scale rearrangements. Genome Biol Evol. **2010**; 2:102–116.
19. Linz B, Ivanov YV, Preston A, et al. Acquisition and loss of virulence-associated factors during genome evolution and speciation in three clades of Bordetella species. BMC Genomics. **2016**; 17(1):767.
20. Bolotin E, Hershberg R. Gene Loss Dominates As a Source of Genetic Variation within Clonal Pathogenic Bacterial Species. Genome Biol Evol. **2015**; 7(8):2173–2187.
21. Albalat R, Cañestro C. Evolution by gene loss. Nat Rev Genet. **2016**; 17(7):379–391.
22. Trouillet-Assant S, Lelièvre L, Martins-Simões P, et al. Adaptive processes of Staphylococcus aureus isolates during the progression from acute to chronic bone and joint infections in patients. Cell Microbiol. **2016**; 18(10):1405–1414.
23. Chaveroche MK, Ghigo JM, Enfert C d'. A rapid method for efficient gene replacement in the filamentous fungus Aspergillus nidulans. Nucleic Acids Res. **2000**; 28(22):E97.
24. Colucci-Guyon E, Tinevez J-Y, Renshaw SA, Herbomel P. Strategies of professional phagocytes in vivo: unlike macrophages, neutrophils engulf only surface-associated microbes. J Cell Sci. **2011**; 124(Pt 18):3053–3059.
25. Deatherage DE, Barrick JE. Identification of mutations in laboratory evolved microbes from next-generation sequencing data using breseq. Methods Mol Biol. **2014**; 1151:165–188.
26. Garrison E, Marth G. Haplotype-based variant detection from short-read sequencing [Internet]. arXiv; 2012 [cited 2023 Oct 16]. Available from: http://arxiv.org/abs/1207.3907

462 27. Ghalayini M, Launay A, Bridier-Nahmias A, et al. Evolution of a Dominant Natural
463 Isolate of Escherichia coli in the Human Gut over the Course of a Year Suggests a Neutral
464 Evolution with Reduced Effective Population Size. Appl Environ Microbiol. **2018**;
465 84(6):e02377-17.
466 28. Wickham H. ggplot2: Elegant Graphics for Data Analysis [Internet]. New York, NY:
467 Springer; 2009 [cited 2023 Feb 7]. Available from: https://link.springer.com/10.1007/978-0-
468 387-98141-3
469 29. Wiles TJ, Bower JM, Redd MJ, Mulvey MA. Use of Zebrafish to Probe the Divergent
470 Virulence Potentials and Toxin Requirements of Extraintestinal Pathogenic Escherichia coli.
471 PLOS Pathogens. Public Library of Science; **2009**; 5(12):e1000697.
472 30. Giraud A, Matic I, Tenaillon O, et al. Costs and benefits of high mutation rates:
473 adaptive evolution of bacteria in the mouse gut. Science. **2001**; 291(5513):2606–2608.
474 31. Tenaillon O, Barrick JE, Ribeck N, et al. Tempo and mode of genome evolution in a
475 50,000-generation experiment. Nature. **2016**; 536(7615):165–170.
476 32. Svensson Malchau K, Tillander J, Zaborowska M, et al. Biofilm properties in relation
477 to treatment outcome in patients with first-time periprosthetic hip or knee joint infection. J
478 Orthop Translat. **2021**; 30:31–40.
479 33. Sanchez CJ, Mende K, Beckius ML, et al. Biofilm formation by clinical isolates and
480 the implications in chronic infections. BMC Infect Dis. **2013**; 13:47.
481 34. Post V, Harris LG, Morgenstern M, et al. Comparative Genomics Study of
482 Staphylococcus epidermidis Isolates from Orthopedic-Device-Related Infections Correlated
483 with Patient Outcome. J Clin Microbiol. **2017**; 55(10):3089–3103.
484 35. Smith KD, Andersen-Nissen E, Hayashi F, et al. Toll-like receptor 5 recognizes a
485 conserved site on flagellin required for protofilament formation and bacterial motility. Nat
486 Immunol. **2003**; 4(12):1247–1253.
487 36. Bambou J-C, Giraud A, Menard S, et al. In vitro and ex vivo activation of the TLR5
488 signaling pathway in intestinal epithelial cells by a commensal Escherichia coli strain. J Biol
489 Chem. **2004**; 279(41):42984–42992.
490 37. Giraud A, Arous S, De Paepe M, et al. Dissecting the genetic components of
491 adaptation of Escherichia coli to the mouse gut. PLoS Genet. **2008**; 4(1):e2.
492 38. Leatham MP, Stevenson SJ, Gauger EJ, et al. Mouse intestine selects nonmotile flhDC
493 mutants of Escherichia coli MG1655 with increased colonizing ability and better utilization of
494 carbon sources. Infect Immun. **2005**; 73(12):8039–8049.
495 39. Winstanley C, O'Brien S, Brockhurst MA. Pseudomonas aeruginosa Evolutionary
496 Adaptation and Diversification in Cystic Fibrosis Chronic Lung Infections. Trends Microbiol.
497 **2016**; 24(5):327–337.
498 40. Viberg LT, Sarovich DS, Kidd TJ, et al. Within-Host Evolution of Burkholderia
499 pseudomallei during Chronic Infection of Seven Australasian Cystic Fibrosis Patients. mBio.
500 **2017**; 8(2):e00356-17.
501 41. Moran NA. Microbial minimalism: genome reduction in bacterial pathogens. Cell.
502 **2002**; 108(5):583–586.
503 42. Weinert LA, Welch JJ. Why Might Bacterial Pathogens Have Small Genomes? Trends
504 Ecol Evol. **2017**; 32(12):936–947.
505 43. D'Souza G, Kost C. Experimental Evolution of Metabolic Dependency in Bacteria.
506 PLoS Genet. **2016**; 12(11):e1006364.
507 44. Tay WH, Chong KKL, Kline KA. Polymicrobial-Host Interactions during Infection. J
508 Mol Biol. **2016**; 428(17):3355–3371.
509 45. Boldock E, Surewaard BGJ, Shamarina D, et al. Human skin commensals augment
510 Staphylococcus aureus pathogenesis. Nat Microbiol. **2018**; 3(8):881–890.
511

Figure legends

Figure 1. Biofilm formation capacity for infection and relapse strains from case 1 (**A**), 2 (**B**) and 3 (**C**). Six different surfaces were tested, *E. coli* K12 MG1655 was used as a control for weak biofilm formation and *E. coli* TG1 as a control for strong biofilm formation (n=3 to 4 biological replicates). (**D**) Adhesion capacity on osteoblast human cells (n=3 biological replicates). For each panel, statistical significance was only assessed between the infection strain and its related relapse strain according to non-parametric two-tailed Mann-Whitney test. * $p<0.05$; ** $p<0.01$.

Figure 2. Serum survival capacity. **A**. Normalized serum survival capacity of each strain expressed as percentage of the control for growth in Heat Inactivated Serum (HIS). *E. coli* strains CFT073 and MG1655 were used as positive and negative controls, respectively (n=3 biological replicates). Statistical significance was only assessed between the infection strain and its related relapse strain according to non-parametric two-tailed Mann-Whitney test. * $p<0.05$. **B**. LPS profile of I2 and R2 strains. *E. coli* MG1655 was used as a negative control and the same strain in which the O-Antigen was reconstructed was used as a positive control. **C**. Relative Serum survival of I2 ancestral strain, R2 relapse strain as well as two deletion mutants constructed in the I2 ancestral strain: one for the *afa* fimbrial operon and a second for the *yadA*-like encoding gene. Results are expressed relatively to R2 relapse strain (n=4 biological replicates). Statistical significance according to non-parametric two-tailed Mann-Whitney test. * $p<0.05$; ** $p<0.01$.

Figure 3. Virulence of the strains. (**A**) Cytotoxicity test on HeLa cells. All six adapted and ancestral strains were tested as well as MG1655 strain as a negative control. The values for each strain were expressed relatively to the control without bacteria (n=3 biological replicates). No statistical significance was detected according to non-parametric two-tailed Mann-Whitney test. (**B**) Hemolysis capacity in liquid culture of each relapse strain relatively to its ancestor (n=3 biological replicates). Values higher than 1 show higher hemolysis capacity for the relapse strain, while values lower than 1 show lower hemolysis capacity for the relapse strain. Statistical significance according to non-parametric two-tailed Mann-Whitney test. * $p<0.05$. (**C**) Monitoring of zebrafish survival (no statistical significance was detected according to log-rank test), (**D**) bacterial burden into the zebrafish (no statistical significance was detected according to non-parametric two-tailed Mann-Whitney test) and (**E**) *in vivo* fluorescence of macrophages and neutrophils for zebrafish infected by I2 and R2 strains as well as non-injected

control, MG1655 strain (negative control) and CFT073 (positive control). Each image is representative of 5 biological replicates. Fifteen zebrafish were used for each experiment in C and D.

Figure 4. Fitness competitions and growth capacities. (**A)** Fitness competitions of relapse against ancestral strain for all three pairs in planktonic and biofilm conditions (n=6 biological replicates). Statistical significance according to non-parametric two-tailed Mann-Whitney test (*: p-value < 0.05, **: p-value < 0.01). (**B)** Fitness competitions of R2 relapse strain against I2 ancestral strain in different conditions (same as in supplementary Figure S6.B-F). BIP: 2,2'-Bipyridyl (n=6 biological replicates). Statistical significance according to non-parametric two-tailed Mann-Whitney test (*: p-value < 0.05).

Supplementary Figures legends

Supplementary Figure 1. Optimization of competition protocols. (**A**) Assessment of the fitness cost associated to the expression of each fluorescence marker (GFP or mars) in each strain (n=3 biological replicates). There is a slight cost to produce mars marker in I3 and R3 strains as compared to the production of GFP. Therefore, both combinations of fluorescence marker were used in the competition assays for all strains. Statistical significance according to two-tailed Mann-Whitney test comparing initial and relapsing strains (*: p-value < 0.05, **: p-value < 0.01). (**B**) Comparison of FACS approach and Sanger based QSVanalyzer approach to assess the proprotion of each strain in a set of mixed samples with different proportions of I1 and R1 strains taged with GFP and mars, respectively (n=3 biological replicates).

Supplemental Figure 2. Motility of each strain assessed on low agar plates at 30 and 37°C. A *E. coli* MG1655 strain deleted for fliE to fliR genes is used as a negative control and a *E. coli* MG1655 strain in which the motility is increased by the insertion of an IS1 in *yeaJ/dgcJ* encoding a diguanylate cyclase resulting in an increase of c-di-GMP, which in turn fuels motility was used as a positive control.

Supplementary Figure 3. Influence of temperature on I1 and R1 strain motility. Motility of each strain at 30°C (**A**) or 37°C (**B**) when pre-cultured in liquid at 30°C or 37°C. (**C**) Motility of each strain deleted for *fliC* when pre-cultured at 30°C or 37°C and incubated at 30°C for motility testing. (**D**) Production of flagellin (top panel) and RNA polymerase alpha subunit used as a loading control (bottom panel) in I1 and R1 strains assessed by Western blot analysis in different combinations of temperature in liquid cultures.

Supplementary Figure 4. **A**. Auto-aggregation kinetic of all clinical strains. In each case, the infection strain is compared to the relapse strain as well as a strain of *E. coli* MG1655 in which *flu* is under the control of a constitutive promoter (PCL-flu) used as a positive control and a strain of *E. coli* MG1655 in which *flu* is deleted (Δflu) used as a negative control (n=3 biological replicates). No statistical significance was identified according to two-tailed Mann-Whitney test comparing initial and relapsing strains. **B**. Pictures showing the red, dry, and rough (rdar) morphotypes of each strain after 24 or 48 hours of incubation at either 30°C or 37°C. The first couple had a pink, dry and rough (pdar) morphotype characterizing the production of curli only. The second couple had a smooth and white morphotype (saw) showing the absence of matrix component production. The third couple had pink and smooth morphotype (pas) showing the production of cellulose only.

Supplementary Figure 5. Zebrafish *in vivo* experiments. Monitoring of zebrafish survival (left panel) and bacterial burden into the zebrafish (right panel) for I1 and R1 (**A**), I2 and R2 (**B**) and I3 and R3 (**C**). MG1655 strain was used as a negative control and CFT073 strain as a positive control. Fifteen zebrafish were used for each experiment and no significant statistical different was identified between the infection strains and their relative relapse strains according to log-rank test for the survival and two-tailed Mann-Whitney test for the bacterial burden comparing initial and relapsing strains.

Supplementary Figure 6. Growth capacities in different conditions. (**A)** Growth curve and related parameters inferred by the R package GrowthCurver (values for which the difference between both strains was significant (two-tailed Mann-Whitney test, p-value < 0.05) are highlighted in bold red) for I1 and R1 strains grown in M63B1 minimum medium supplemented with 0.4% pyruvate (n=5 biological replicates). (**B-F)** Growth curve and related parameters inferred by the R package GrowthCurver (values for which the difference between both strains was significant (two-tailed Mann-Whitney test, p-value < 0.05) are highlighted in bold red) for I2 and R2 strains grown in M63B1 minimum medium supplemented with 0.4% lactate (B), Maltose (C), Glucose (D) as well as in LB medium (E) and LB medium supplemented with 500 µM of 2,2'-Bipyridyl (F) (n=5 biological replicates).

Supplemental Figure 7. Colicin production in R1 relapse strain. **A**. Overlay of R1 strain showing no growth inhibition by a drop of either I1 or R1 supernatant from a culture in presence of Mitomycin C to induce colicin production. **B**. Same experiment with an overlay of I1 strain showing a growth inhibition by a drop of R1

supernatant from a culture in presence of Mitomycin C to induce colicin production. In both cases, LB is used as a negative control.

Table 1. Cases and strain information. Table summarizing the type and location of infection as well as type of sample. Each strain was typed *in silico* and, when the infection was polymicrobial, the other species involved are listed. ANI: Average Nucleotide Identity, MLST: MultiLocus Sequencing Typing.

Case N°	Strain	Infection status	Infection site	Sample type	Diagnosis	Time before relapse	Antibiotic susceptibility profile	Phylogroup	Serotype	ANI	MLST #1	MLST #2	fimH	fumC	Infection type	Other pathogens if polymicrobial
1	I1	Initial	Hand	Deep tissue by swab	Septic arthritis 4th finger (no material)	51 days	Penicillinase	B1	O76:H28	99.99%	224	730	FimH39	FumC4	Monomicrobial	
	R1	relapse		Deep tissue by swab			Identical								Polymicrobial	*Enterococcus faecium*, *Pseudomonas aeruginosa*, *Citrobacter freundii*
2	I2	Initial	Spine	Washing liquid	Vertebral osteomyelitis (no material)	748 days	ESBL-producing	G	O24:H4	99.99%	117	48	FimH97	FumC45	Monomicrobial	
	R2	relapse		biopsy			Identical								Polymicrobial	*Cutibacterium acnes*
3	I3	Initial	Right hip	Bone	Prosthetic joint infection	66 days	ESBL-producing	A	O89/O162:H9	99.99%	167	2	/	FumC11	Monomicrobial	
	R3	relapse		Deep tissue			Identical								Monomicrobial	

Table 2. SNP analysis in the relapse strains. SNPs, insertions and deletions identified in the evolved strains as compared to their related ancestor.

Strain	Mutation	Supporting reads (Left/Right)	Annotation	Impact	Gene	Description
R1	T→A	104 / 83	intergenic (+168/-221)	Intergenic	uidR → / → uidA	transcriptional repressor/beta-D-glucuronidase
	A→G	191 / 136	N16D (AAC→GAC)	Non-synonymous	yehT →	putative response regulator in two-component system withYehU
	T→C	273 / 260	T46A (ACA→GCA)	Non-synonymous	rppH ←	RNA pyrophosphohydrolase
	T→C	129 / 119	K577E (AAG→GAG)	Non-synonymous	ydiJ ←	putative FAD-linked oxidoreductase
R2	G→A	152 / 189	G335G (GGC→GGT)	Synonymous	COMLMOEC_00122 ←	hypothetical protein
	C→G	56 / 52	V16L (GTA→CTA)	Non-synonymous	insK_3 ←	IS150 transposase B
	C→G	62 / 82	S67T (AGC→ACC)	Non-synonymous	COMLMOEC_04582 ←	IS3 family transposase IS629
	C→T	265 / 166	A131T (GCC→ACC)	Non-synonymous	ebgR ←	transcriptional repressor
	C→T	172 / 171	A197V (GCC→GTC)	Non-synonymous	COMLMOEC_04752 →	IS66 family transposase ISEc47
	T→A	86 / 55	I263N (ATT→AAT)	Non-synonymous	btuC →	vitamin B12 ABC transporter permease
	A→G	164 / 169	intergenic (+1283/–)	Intergenic	COMLMOEC_01687 → / –	hypothetical protein/–
	A→C	66 / 84	intergenic (+352/–)	Intergenic	COMLMOEC_04947 → / –	hypothetical protein/–
R3	G→T	146 / 182	E297D (GAG→GAT)	Non-synonymous	hypT →	hypochlorite-responsive transcription factor
	G→A	73 / 103	D119N (GAT→AAT)	Non-synonymous	insF1_1 →	IS3 transposase B
	C→T	56 / 61	intergenic (+315/-76)	Intergenic	uidR → / → uidA	transcriptional repressor/beta-D-glucuronidase
	Δ1 bp	59 / 71	intergenic (-142/+229)	Intergenic	araD ← / ← araA	L-ribulose-5-phosphate 4-epimerase/L-arabinose isomerase

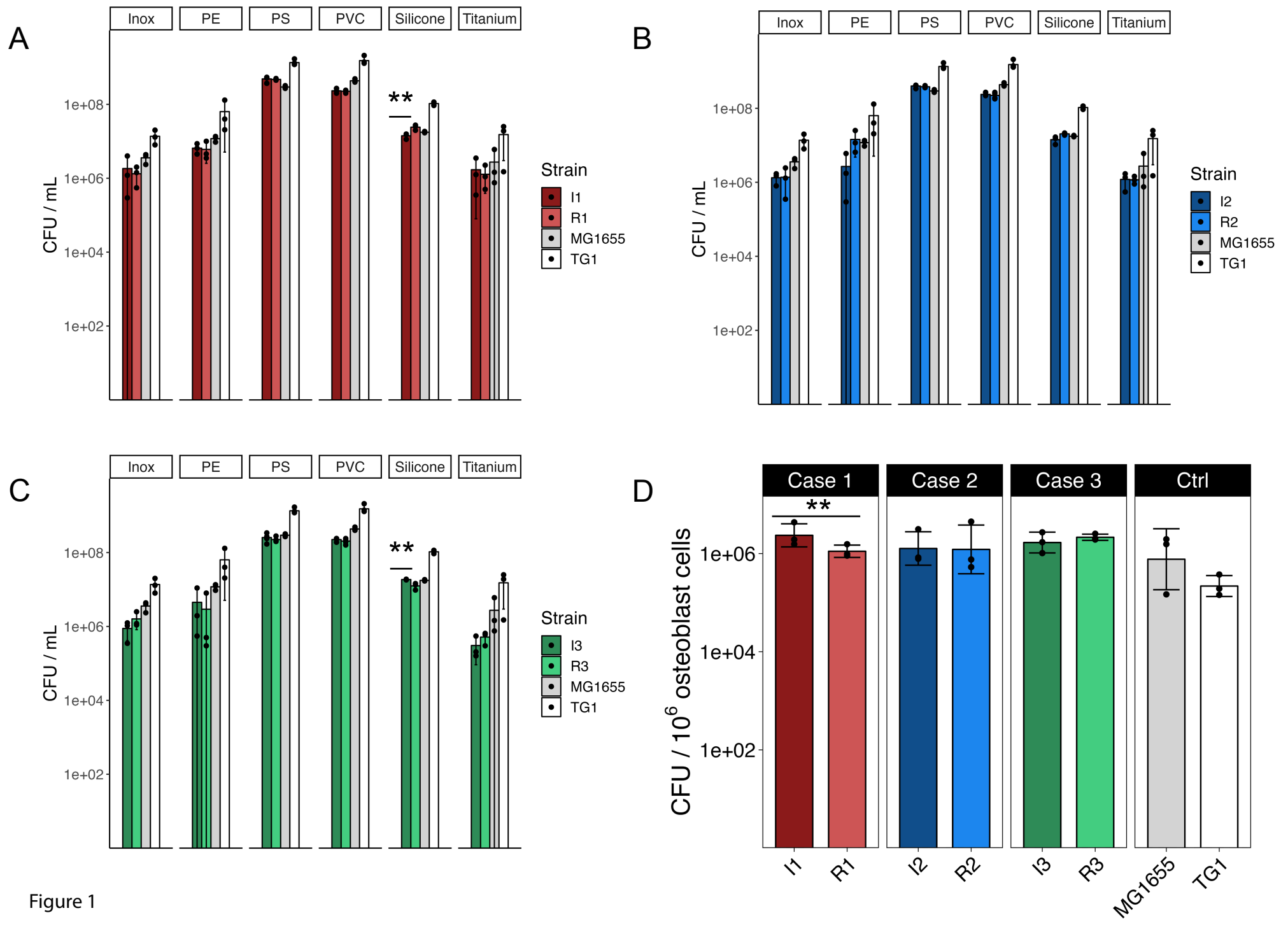
A
Inox
PE
PS
PVC
Silicone
Titanium
CFU / mL
1e+08
1e+06
1e+04
1e+02
**
Strain
I1
R1
MG1655
TG1
B
Inox
PE
PS
PVC
Silicone
Titanium
CFU / mL
1e+08
1e+06
1e+04
1e+02
Strain
I2
R2
MG1655
TG1
C
Inox
PE
PS
PVC
Silicone
Titanium
CFU / mL
1e+08
1e+06
1e+04
1e+02
**
Strain
I3
R3
MG1655
TG1
D
Case 1
Case 2
Case 3
Ctrl
**
CFU / 10^6 osteoblast cells
1e+06
1e+04
1e+02
I1
R1
I2
R2
I3
R3
MG1655
TG1

Figure 1

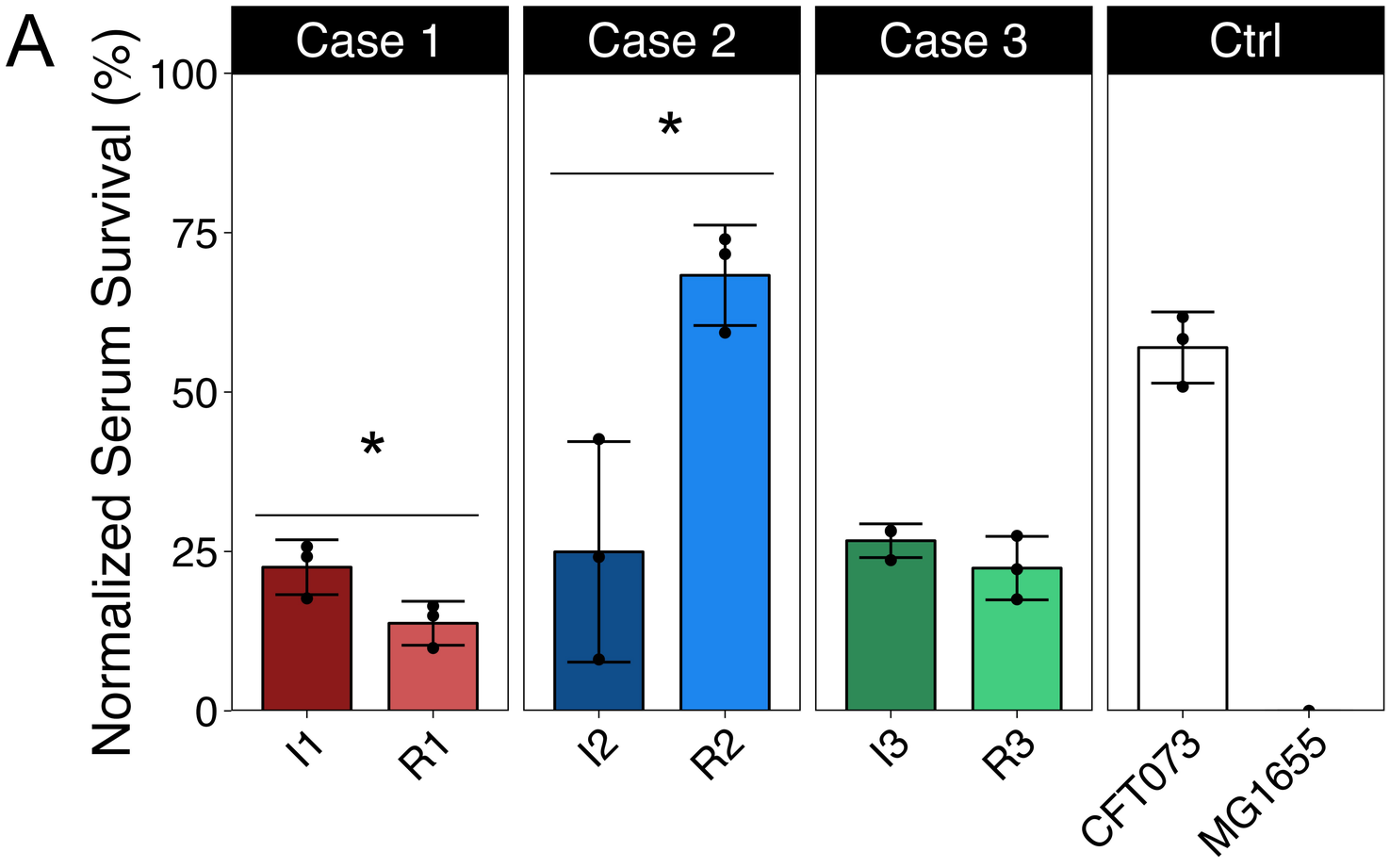
A
Case 1
Case 2
Case 3
Ctrl
Normalized Serum Survival (%)
100
75
50
25
0
*
*
I1
R1
I2
R2
I3
R3
CFT073
MG1655

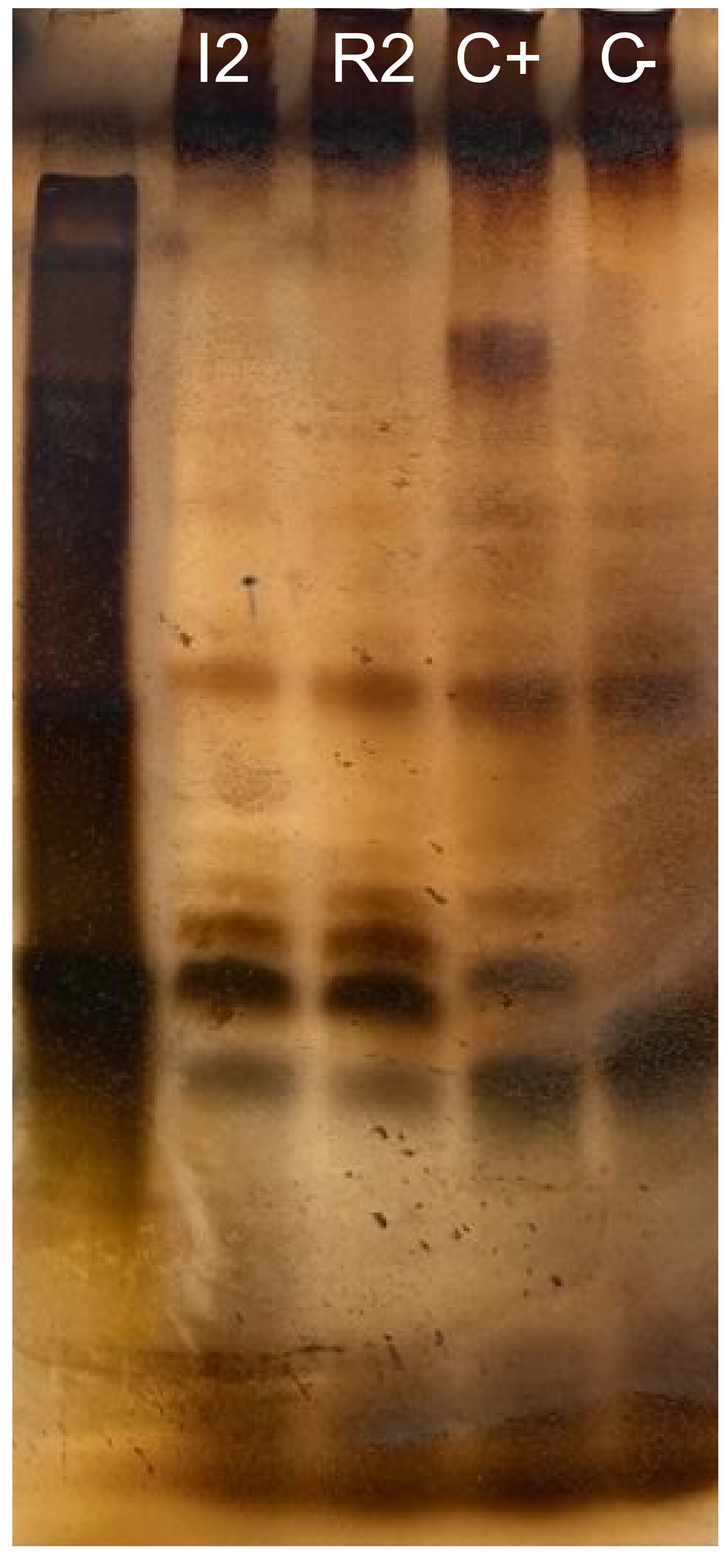
B
I2
R2
C+
C-

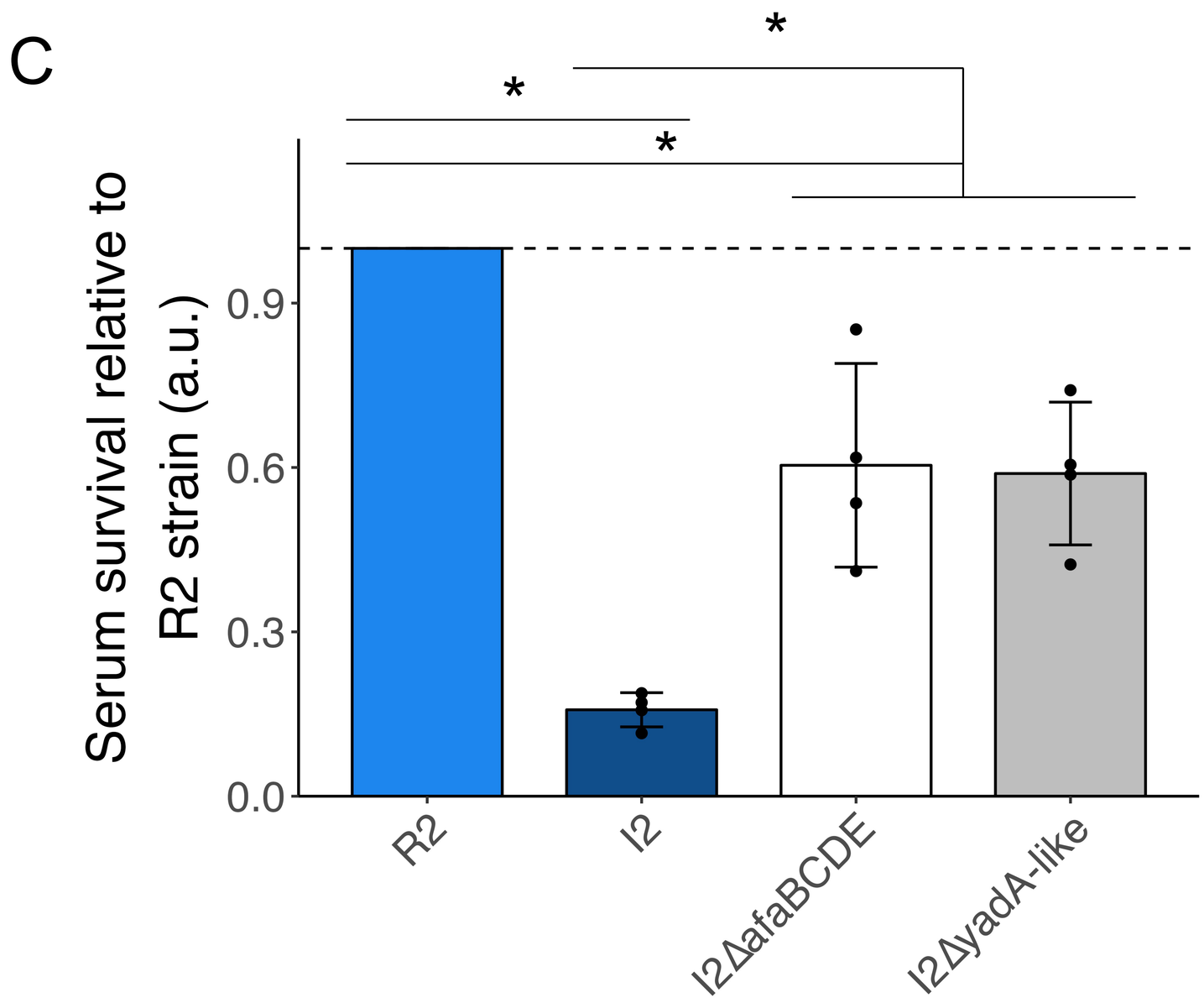
C
*
*
*
Serum survival relative to
R2 strain (a.u.)
0.9
0.6
0.3
0.0
R2
I2
I2ΔafaBCDE
I2ΔyadA-like

Figure 2

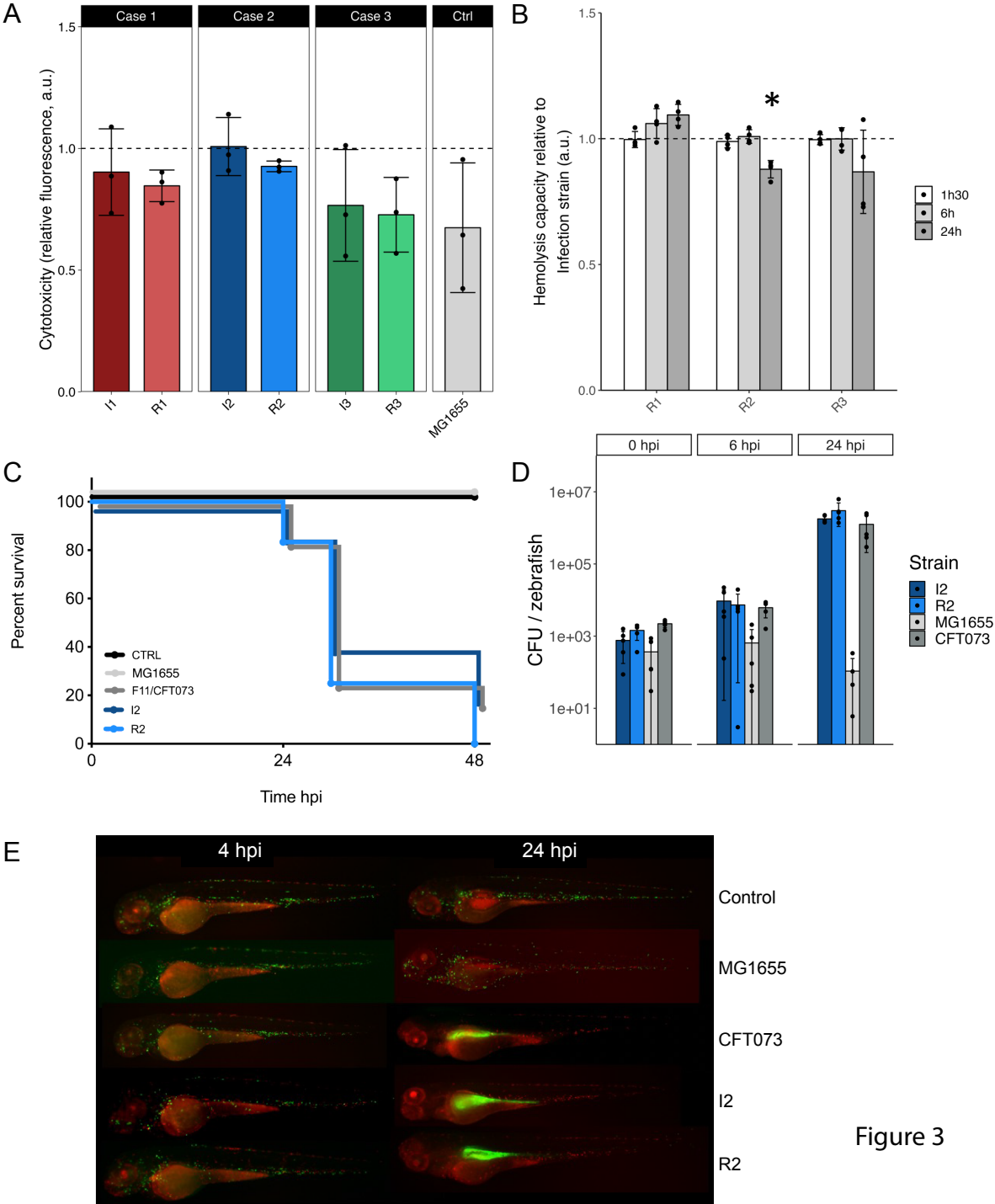
A
Case 1
Case 2
Case 3
Ctrl
Cytotoxicity (relative fluorescence, a.u.)
1.5
1.0
0.5
0.0
I1
R1
I2
R2
I3
R3
MG1655
B
Hemolysis capacity relative to Infection strain (a.u.)
*
1h30
6h
24h
R1
R2
R3
C
Percent survival
100
80
60
40
20
0
CTRL
MG1655
F11/CFT073
I2
R2
0
24
48
Time hpi
D
0 hpi
6 hpi
24 hpi
CFU / zebrafish
1e+07
1e+05
1e+03
1e+01
Strain
I2
R2
MG1655
CFT073
E
4 hpi
24 hpi
Control
MG1655
CFT073
I2
R2

Figure 3

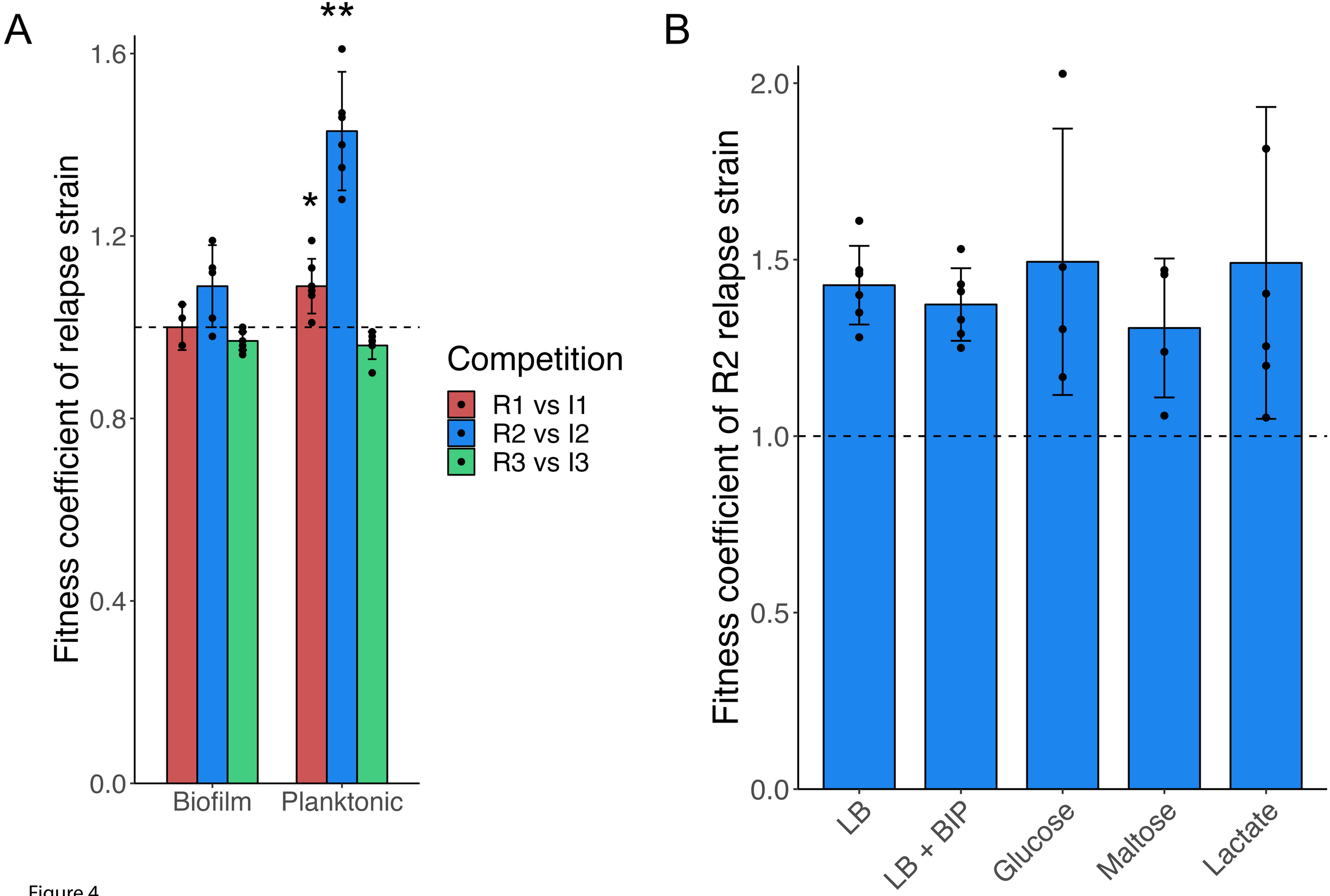
A
B
Fitness coefficient of relapse strain
1.6
1.2
0.8
0.4
0.0
*
**
Biofilm
Planktonic
Competition
R1 vs I1
R2 vs I2
R3 vs I3
Fitness coefficient of R2 relapse strain
2.0
1.5
1.0
0.5
0.0
LB
LB + BIP
Glucose
Maltose
Lactate

Figure 4

Supplementary Table 1. Antibiotic susceptibility profiles. Resistant (R), sensitive (S) or intermediate (I) status of each strain to commonly used antibiotics assessed by disc diffusion assay and following EUCAST breakpoints recommendations.

Antibiotic	**I1**	**R1**	**I2**	**R2**	**I3**	**R3**
Ampicillin	R	R	R	R	R	R
Cefoxitin	S	S	S	S	R	R
Meropenem	S	S	S	S	S	S
Ticarcillin	R	R	R	R	R	R
Ticarcillin + clavulanic acid	S	S	R	R	R	R
Cefepime	S	S	R	R	R	R
Ertapenem	S	S	S	S	S	S
Mecillinam	S	S	S	S	S	S
Cefotaxime	S	S	R	R	R	R
Amoxicillin + clavulanic acid	S	S	R	R	R	R
Ceftazidime	S	S	I	I	R	R
Piperacillin	R	R	R	R	R	R
Tazocillin (Piperacillin + Tazobactam)	S	S	R	R	R	R
Aztreonam	S	S	R	R	R	R
Imipenem	S	S	S	S	S	S
Cefalexin	R	R	S	S	S	S
Tobramycin	S	S	S	S	R	R
Amikacin	S	S	S	S	S	S
Norfloxacin	R	R	S	S	R	R
Moxifloxacin	R	R	S	S	R	R
Ciprofloxacin	R	R	S	S	R	R
Co-trimoxazole (Trimethoprim + Sulfamethoxazole)	R	R	S	S	R	R
Tigecycline	S	S	S	S	S	S
Fosfomycin	S	S	S	S	S	S
Nitrofurantoin	S	S	S	S	S	S
Cefadroxil	S	S	S	S	S	S

Supplementary Table 2. List of all strains used in this study.

Strain	Genotype, phenotype	Relevant information	Source
MG1655	F- lambda- *ilvG rfb*-50 *rph*-1	E. coli Genetic Stock Center GCSC#6300	Laboratory collection
TG1	F'[*traD*36 *proAB* + *lacI*q *lacZ*DM15] *supE hsd*D5 *thi* Δ(*lac-proAB*)	Strong biofilm former	Laboratory collection
CFT073	*rpoS* -	Human Blood Pyeloneprhitis (ExPEC) B2 K2	[1]
MG1655 KmFRT-*wbbL*+	F- lambda- *ilvG rfb*-50 *rph*-1 *wbbL*+, KmR	LPS O-antigen restored	[2]
MG1655 Δ*fliE-R*	F- lambda- *ilvG rfb*-50 *rph*-1 Δ*fliE-R*::cat, CmR	Non-motile strain	[3]
MG1655 *yeaJ*/*dgcJ* inter	F- lambda- *ilvG rfb*-50 *rph*-1 with and intergenic mutation between *yeaJ* and *dgcJ*	Hyper motile strain	Laboratory collection
55989	tetR	rdar morphotype on congored plates	[4]
MG1655 Δ*csgD*	F- lambda- *ilvG rfb*-50 *rph*-1 Δ*csgD*::*aadA7*, SpecR	No cellulose production	[5]
MG1655 Δ*flu*	F- lambda- *ilvG rfb*-50 *rph*-1 Δ*flu*::*GB*, KmR	No auto-aggregation	[3]
MG1655 PcL*flu*	F- lambda- *ilvG rfb*-50 *rph*-1 KmPcL-*flu*, KmR	Strong auto-aggregation	[6]
MG1655 lATT Zeo-mars	F- lambda- *ilvG rfb*-50 *rph*-1 lATT-*zeo-mars*, ZeoR	Source of Zeo-mars cassette at the lambda site	Laboratory collection
MG1655 lATT Zeo-GFP	F- lambda- *ilvG rfb*-50 *rph*-1 lATT-*zeo-gfpmut3*, ZeoR	Source of Zeo-GFP cassette at the lambda site	Laboratory collection
I1		WT infection strain from case 1	This study
I1 Δ*fliC*	Δ*fliC*::*zeo*, ZeoR	WT with fliC gene deleted, non-motile mutant	This study
I1 lATT Zeo-GFP	lATT-*zeo-gfpmut3*, ZeoR	WT with gfpmut3 gene inserted together with a zeocin resistance cassette at the λatt site under λPR constitutive promoter	This study
I1 lATT Zeo-mars	lATT-*zeo-mars*, ZeoR	WT with mars gene inserted together with a zeocin resistance cassette at the λatt site under λPR constitutive promoter	This study
R1		WT relapse strain from case 1	This study
R1 Δ*fliC*	Δ*fliC*::zeo, ZeoR	WT with fliC gene deleted, non-motile mutant	This study
R1 lATT Zeo-GFP	lATT-*zeo-gfpmut3*, ZeoR	WT with gfpmut3 gene inserted together with a zeocin resistance cassette at the λatt site under λPR constitutive promoter	This study
R1 lATT Zeo-mars	lATT-*zeo-mars*, ZeoR	WT with mars gene inserted together with a zeocin resistance cassette at the λatt site under λPR constitutive promoter	This study
I2		WT infection strain from case 2	This study
I2 Δ*yadA*-like	Δ*yadA-like*::*zeo*, ZeoR	WT with yadA-like coding gene deleted	This study
I2 Δ*afaBCDE*	Δ*afaBCDE*::*zeo*, ZeoR	WT with genes afaBCDE deleted	This study
R2		WT relapse strain from case 2	This study

I3		WT infection strain from case 3	This study
I3 lATT Zeo-GFP	lATT-*zeo-gfpmut3*, ZeoR	WT with gfpmut3 gene inserted together with a zeocin resistance cassette at the λatt site under λPR constitutive promoter	This study
I3 lATT Zeo-mars	lATT-*zeo-mars*, ZeoR	WT with mars gene inserted together with a zeocin resistance cassette at the λatt site under λPR constitutive promoter	This study
R3		WT relapse strain from case 3	This study
R3 lATT Zeo-GFP	lATT-*zeo-gfpmut3*, ZeoR	WT with gfpmut3 gene inserted together with a zeocin resistance cassette at the λatt site under λPR constitutive promoter	This study
R3 lATT Zeo-mars	lATT-*zeo-mars*, ZeoR	WT with mars gene inserted together with a zeocin resistance cassette at the λatt site under λPR constitutive promoter	This study

1. Mobley HL, Green DM, Trifillis AL, et al. Pyelonephritogenic Escherichia coli and killing of cultured human renal proximal tubular epithelial cells: role of hemolysin in some strains. Infect Immun. **1990**; 58(5):1281–1289.

2. Rendueles O, Beloin C, Latour-Lambert P, Ghigo J-M. A new biofilm-associated colicin with increased efficiency against biofilm bacteria. ISME J. **2014**; 8(6):1275–1288.

3. Francius G, Polyakov P, Merlin J, et al. Bacterial Surface Appendages Strongly Impact Nanomechanical and Electrokinetic Properties of Escherichia coli Cells Subjected to Osmotic Stress. PLOS ONE. Public Library of Science; **2011**; 6(5):e20066.

4. Mossoro C, Glaziou P, Yassibanda S, et al. Chronic Diarrhea, Hemorrhagic Colitis, and Hemolytic-Uremic Syndrome Associated with HEp-2 Adherent Escherichia coli in Adults Infected with Human Immunodeficiency Virus in Bangui, Central African Republic. J Clin Microbiol. **2002**; 40(8):3086–3088.

5. Da Re S, Ghigo J-M. A CsgD-independent pathway for cellulose production and biofilm formation in Escherichia coli. J Bacteriol. **2006**; 188(8):3073–3087.

6. Da Re S, Le Quéré B, Ghigo J-M, Beloin C. Tight modulation of Escherichia coli bacterial biofilm formation through controlled expression of adhesion factors. Appl Environ Microbiol. **2007**; 73(10):3391–3403.

Supplementary Table 3. List of all primers used in this study.

I1/R1 and I3/R3 lATT Zeo-mars and Zeo-GFP construction and verification	
lambda-ATT. B1.500-3	CCCTGATACTCACCAGGCATCAC
Rev_K12-ZeoXFP-lATT	GTCACGCCAAAAGCCAATGC
Fw_K12-ZeoXFP-lATT	GCAAGCGCCTCGATTACTGC
lambda-ATT.A1.500-5	CGATGGCGATAATATTTCACC
Sanger sequencing-based fitness assessment in I2/R2	
Fw_butC	CAGTCGGTTATTGCTGGCT
Rv_butC	CACACTTTGAGGCGACATTG
Sanger sequencing-based fitness assessment calibration vs FACS in I1/R1	
Fw_yehT	CAACATTTGATGCTGGAGATCG
Rv_yehT	GCTTCATCAATTGGCTTCAGC
afaBCDE deletion in I2 and verification	
Fw_afaDel_size_ZeoFRT	GATTCAGCACCTCAGTCAGAC
Fw_Del_afaB-E_ZeoFRT	GGTTGCTATTAACATATTTATAAAAGGTTTATTTGCCTTCAGGATAAAATATGTAGGCTGGAGCTGCTTC
Rv_Del_afaB-E_ZeoFRT	CAAAGGGAGCATATAGCCCCCTTCTTTCATCAGGTTAATTTTCCAGAATATCCTCCTTAGTTCCTATTCC
Rv_afaDel_size_ZeoFRT	GCGAGGAAGATTTCTCTTGTAGG
yadA-like deletion in I2 and verification	
Fw_Size_yadA_Del	TGCTGCTTAAATTGAGGTCGC
Fw_Del_yadA_ZeoFRT	CTCCGCACTACCGTTCTGGCTGGTGAAGTAATAATACAGGAGAATAACAGATGTAGGCTGGAGCTGCTTC
Rv_Del_yadA_ZeoFRT	TCCCGGGGGACTCCCCCCGGGACAGATATCTAAATCCTGACCTGGAATATCCTCCTTAGTTCCTATTCCG
Rev_Size_yadA_Del	CGATTCCAAATATCTCTCGCAGG
fliC deletion in I1/I2 and verification	
Fw_fliC	GGCATGATTATCCGTTTCTGC
Fw_CmFRT_ForFliC	TTGGCGTTGCCGTCAGTCTCAGTTAATCAGGTTACAACGAATTTAAATGGCGCGCCTTAC
Rev_CmFRT_ForFliC	CCCAATACGTAATCAACGACTTGCAATATAGGATAACGAATCGCCTACCTGTGACGGAAG
Rev_fliC	TCCCAGCGATGAAATACTTGC

Supplementary Table 4. Genome assembly characteristics and metrics. Table showing data related to sequencing data, genome assembly quality and description.

Case N°	Strain	Read number	Genome coverage average (SD)	Genome size (base pairs)	Contig number	GenBank Assembly accession	N50	L50	GC%	Complete BUSCOs	CDS	Potential plasmid gain	Potential plasmid loss	CDS gained	CDS lost	Mutation per base per year
1	I1	5,761,693	336 (170)	5,124,061	105	JARFPI000000000	193,231	9	50.81	440/440	4,740	n.a				
	R1	7,181,866	418 (200)	5,133,911	97	JARFPF000000000	193,231	10	50.81	440/440	4,754	1	0	35	19	$8.38x10^{-6}$
2	I2	5,591,377	316 (144)	5,300,036	130	JARFPH000000000	194,756	9	50.69	440/440	4,914	n.a				
	R2	5,271,593	308 (132)	5,122,701	111	JARFPE000000000	208,913	8	50.77	440/440	4,775	0	1	31	170	$1.11x10^{-6}$
3	I3	5,594,583	341 (138)	4,900,901	99	JARFPG000000000	137,146	11	50.79	440/440	4,511	n.a				
	R3	4,748,473	289 (118)	4,904,465	98	JARFPD000000000	137,146	11	50.79	440/440	4,518	1	0	14	9	$4.51x10^{-6}$

Analysis of *in-patient* evolution of *Escherichia coli* reveals potential links to relapse of bone and joint infections

Stanislas THIRIET-RUPERT[1], Jérôme JOSSE[2], David PEREZ-PASCUAL[1], Jason TASSE[2], Camille ANDRE[2], Lélia ABAD[2], David LEBEAUX[1], Jean-Marc GHIGO[1], Frédéric LAURENT[2] and Christophe BELOIN*[1]

Supplementary Results

Auto-aggregation and RDAR morphotypes on congo-red plates

Once settled and in order to colonize host environment, *E. coli* has a very large arsenal of adhesion factors. Some of them are known to promote biofilm formation via homotypic self-interactions also called auto-aggregation [1,2], which could help facing stressful conditions such as the one encountered in vivo. The production of other factors such as curli and cellulose are also of critical importance [3,4] and induces a red, dry, and rough (rdar) morphotype when the strain is plated on LB agar supplemented with congo red. However, none of these phenotypes showed any difference when comparing the relapse strains to their related ancestors, all strains even having very weak auto-aggregation capacities (supplementary Figure S1.A.B). Still, inter-couple differences were identified on congo red plates: (i) the first couple had a pink, dry and rough (pdar) morphotype characterizing the production of curli only; (ii) the second couple had a smooth and white morphotype (saw) showing the absence of matrix component production; and (iii) the third couple had pink and smooth morphotype (pas) showing the production of cellulose only.

Temperature specific motility

Because strain motility could have an impact on the virulence and biofilm forming capacity, we tested each strain on LB plates containing low amount of agar at 30°C and 37°C. Motility is sometime more visible at lower temperature. The second and third couple strains had no motility (supplemental Figure S2). However, an interesting phenotype was observed for the first couple. Although both strains were motile, we observed some flares characteristic of the apparition of a hypermotile clone within the population and spreading faster than the others (supplementary Figure S2). Because this phenomenon was only observed at 37°C, we investigated the importance of temperature by testing all combinations between the temperature used to produce the liquid inoculum and the temperature the motility plates were incubated at. We showed that regardless of the temperature used for the liquid culture, incubating the motility plate at 30°C always showed a homogenous motile phenotype, while plates inoculated with the same samples but incubated at 37°C always showed the apparition of flares (supplementary Figure S3.A.B.C). This suggests that the process is reversible and a westernblot analysis using anti-flagellin antibodies showed that both strains only produce flagellin at 30°C, even when pre-incubated at 37°C (supplementary Figure S3.D). Therefore, it seems that some mutants arise on plates incubated at 37°C in which the capacity to swim is restored.

Because the apparition of hyper-motile mutants suggests a high mutation rate, we used a Luria-Delbruck fluctuation test to evaluate it. Resistance to Rifampicin was used in these assays and strains I1 and R1 had a mutation rate of 1.58×10^{-6} and 1.39×10^{-6} mutations per generation, respectively, which was by far higher than MG1655 as estimated in the same assay (3.21×10^{-8} mutations per generation), which was in accordance with what was reported in the literature for the same kind of experiment in Escherichia coli K12 MG1655 (see Figure 4 from [5]). Such a high mutation rate could be the result of a loss of function in genes responsible for DNA repair

such as the mut genes. However, no such loss of function could be identified in the genome of the clinical strains.

Genome analysis

To confirm that in each case the relapse strain was the same as the initial infection one all of them were subjected to whole genome sequencing (WGS) and the genomic characteristics analyzed. Each case showed that both strains were indeed the same according to their phylogroup, serotype, ANI, MLST, FimH and FumC type (Table 1).

If the genome assemblies and completeness were good for all strain, the first notable difference identified between the infection strains and their related relapse strains was the number of gained and lost genes (supplementary Table S4). Some of these genes corresponded to a whole contig that matched known plasmids, therefore constituting potential gain or loss of plasmids (supplementary Data 2). R1 relapse strain gained a potential plasmid bearing Colicin E1 production genes, R2 relapse strain lost a potential plasmid containing hypothetical protein coding genes and R3 relapse strain gained a potential plasmid containing a Toxin/Antitoxin (T/A) system (HigA/HigB). However, PacBio sequencing technology would be required to rule out what proportion of the gene gains and losses was plasmid-mediated or the consequence of big chromosomic insertions or deletions.

References

1. Kjaergaard K, Schembri MA, Ramos C, Molin S, Klemm P. Antigen 43 facilitates formation of multispecies biofilms. Environ Microbiol. **2000**; 2(6):695–702.
2. Danese PN, Pratt LA, Dove SL, Kolter R. The outer membrane protein, antigen 43, mediates cell-to-cell interactions within Escherichia coli biofilms. Mol Microbiol. **2000**; 37(2):424–432.
3. Gualdi L, Tagliabue L, Bertagnoli S, Ieranò T, De Castro C, Landini P. Cellulose modulates biofilm formation by counteracting curli-mediated colonization of solid surfaces

in Escherichia coli. Microbiol Read Engl. **2008**; 154(Pt 7):2017–2024.
4. Beloin C, Roux A, Ghigo JM. Escherichia coli biofilms. Curr Top Microbiol Immunol. **2008**; 322:249–289.
5. Krašovec R, Richards H, Gifford DR, et al. Opposing effects of final population density and stress on Escherichia coli mutation rate. ISME J. Nature Publishing Group; **2018**; 12(12):2981–2987.

Analysis of *in-patient* evolution of *Escherichia coli* reveals potential links to relapse of bone and joint infections

Stanislas THIRIET-RUPERT[1], Jérôme JOSSE[2], David PEREZ-PASCUAL[1], Jason TASSE[2], Camille ANDRE[2], Lélia ABAD[2], David LEBEAUX[1], Jean-Marc GHIGO[1], Frédéric LAURENT[2] and Christophe BELOIN*[1]

Supplementary Methods

RDAR morphotypes on congo red plates

Two microliters of an overnight culture grown at 37°C in LB medium under shaking (with appropriate antibiotics when needed) was spotted onto LB plates (without NaCl) containing 0.004% Congo Red and 0.002% brilliant blue. The spotted drops were allowed to dry, and the plates were incubated for 24 and 48 hours at 30 or 37°C.

Auto-aggregation curves

Cultures were grown as described above, and 1mL aliquots were diluted to an OD_{600}=3 in spent medium in order to prevent growth during experiment. Once diluted, all the tubes were vortexed and an aliquot of 50µL was removed, 1cm below the top of the culture, and diluted with 50µL of LB prior to OD_{600} measurement. The bacteria were then left to aggregate at RT for 6 hours, while repeating the measurement of OD_{600} 1 cm below the top of the culture every hour.

Motility assay

Bacterial strains were incubated overnight in LB at the specified temperature with shaking. Then, 2µL of overnight culture was inoculated in swim plates (1% tryptone, 0.25% NaCl, 0.25%

Eiken agar) for 24 hours at 37°C or 30°C. After incubation, motility was assessed by checking the spread of inoculated bacteria into the motility agar.

Biofilm microtiter plate CV assay

Bacteria were grown overnight and diluted to an OD_{600}=0.05 and 100µL were inoculated in technical triplicates in either a polystyrene Greiner 96-well plate or a polyvinyl chloride (PVC) round bottom 96-well plates (Corning). After 24 hours at 37°C, the biofilms were washed twice by slowly pipetting PBS in each well to remove non-attached bacteria. Biofilms were then resuspended in 100µL of PBS by vigorous pipetting and viable cell count was determined by serial dilution and plating.

Growth capacity

An overnight culture of each strain was diluted to OD_{600} of 0.05 in appropriate medium. One hundred and fifty µL aliquots were inoculated in a 96-well plate. The plates were then incubated in a TECAN Infinite M200 Pro spectrophotometer (Männedorf, Switzerland) for 18 hours at 37°C with shaking of 2mm amplitude. The absorbance of each culture at 600 nm was measured every 15 minutes. Growth curve of each strain was measured using 3 biological replicates.
The R package GrowthCurver [1] was used to infer growth-related parameters for all strains based on the growth curves.

Cytotoxicity on HeLa cells

The cytotoxic activity on Hela cells of each bacterial strain was analyzed using the CellTiter-Blue® Cell Viability Assay (Promega) following manufacturer instructions. HeLa cells were cultured in complete DMEM (Life Technologies) supplemented with 10% FCS, 100µg/mL penicillin/streptomycin, and 10mM L-glutamine at 37C in the presence of 5% CO_2. For

infection assay, the HeLa cells were incubated in 96-well plates to reach a density of 10^5 cells. Each bacterial strain was grown overnight in LB as described above and then washed twice in PBS, to finally adjust the bacterial density to 10^7 CFU/ml. These bacterial suspensions were used to infect HeLa cells by adding 100 µl of each to the wells (MOI of 1:100). The plates were incubated at 37C in the presence of 5% CO_2 for 2 hours. Non-infected cells and the *E. coli* K12 MG1655 strain were used as negative controls. At the end of the incubation time, the wells were washed twice with PBS to remove the bacteria. Then, 100 µl of PBS and 20 µl of CellTiter Blue solution were added to each well and incubated for 2 hours at 37C and 5% CO_2. The cell viability was measured by recording the fluorescence at 560/590 nm using a Tecan Infinite-M200-Pro spectrophotometer.

Hemolysis capacity

The hemolytic activity of each strain was assessed by mixing defibrinated horse blood (bioMerieux, Marcy l'Etoile, France) diluted to 10% (v/v) in PBS with a total of 10^8 bacteria in PBS. After 2, 6 and 24 hours of incubation at 37°C with shacking, the non-lysed erythrocytes were pelleted by centrifugation at 1500g for 2 minutes, and the OD_{450} of 150µL of the cell-free supernatants was measured. The hemolytic capacity of each adapted strain was expressed relatively to its ancestral strain.

Luria-Delbrück fluctuation test

The mutation rate of I1, R1 and MG1655 strains were assessed using Luria-Delbrück fluctuation test [2]. For each strain, 60 wells of a 96-well plate were inoculated with ~100 bacteria in a volume of 200µL in LB before incubating the plate in a humid atmosphere for 16h at 37°C under 450 rpm shaking. After the cultures had reach saturation, ten randomly chosen wells were sampled to evaluate the number of total bacteria per well by serial dilution and plating. The

total volume of each of the remaining 50 wells was plated on individual LB plates supplemented with 2xMICs of Rifampicin to evaluate the number of resistant cells. The colony count was then used to assess the mutation rate by a maximum likelihood approach available on FALCOR web tool (https://lianglab.brocku.ca/FALCOR/) [3].

Zebrafish care and maintenance

Homozygous Tg(*mfap4::mCherryF*) (ump6Tg) [4] Tg(*mpx::GFP*)^{i114} [5] double transgenic fishes were raised in Institut Pasteur zebrafish facility. Eggs were obtained by natural spawning, bleached according to standard protocols, and then kept in Petri dishes containing Volvic spring water and, from 24 hpf onwards, 0.003% 1-phenyl-2-thiourea (PTU) (Sigma-Aldrich) was added to prevent pigmentation. Embryos as well as infected larvae were reared at 28°C. Larvae were anesthetized with 200 µg/mL of buffered tricaine methane sulfonate (MS-222, Sigma-Aldrich) during the injection procedure as well as during *in vivo* imaging and processing for bacterial burden evaluation.

Evaluation of the bacterial burden in infected zebrafish larvae

Infected zebrafish larvae were collected at 0, 24, and 48 hpi and lysed for the evaluation of the bacterial burden as previously described [6]. Each larva was placed in an individual 1.5 mL Eppendorf tube and anesthetized with tricaine (200 µg/mL), washed with 1 mL of sterile water, and placed in 150 µL of sterile water. Larvae were then homogenized using a pestle motor mixer (Argos). Each sample was transferred to an individual well of a 96-well plate and 10 X serial dilutions were performed. For CFU enumeration and to assess plasmid stability

throughout the infection kinetics, serial dilutions of lysates were plated on MacConkey agar plates supplemented with lactose plates and incubated overnight at 37°C.

Visualization of macrophages and neutrophils in infected zebrafish larvae

Visualization of macrophages and neutrophils on living transgenic reporter larvae was performed upon infection as we previously described [7]. Briefly, bright field, GFP, and RFP images of whole living anesthetized larvae were taken using a Leica Macrofluo Z16 APOA (zoom 16:1) macroscope equipped with a Leica PlanApo 2.0 X lens, and a Photometrics CoolSNAP *HQ2* camera. Images were captured using the Metavue software version 7.5.6.0 (MDS Analytical Technologies). After capture of images, larvae were washed and transferred to a new 24-well plate filled with 1mL of fresh water per well and incubated at 28 °C.

Overlay assay colicin

I1 and R1 strains were incubated overnight at 37°C with shaking in LB supplemented with 40 µg/mL of Mitomycin C to induce colicin production. After incubation an overlay of each strain was realized by pouring 6mL of overnight culture diluted at OD_{600}=0.1 onto a LB agar plate and removing it after 5 minutes. Plates were allowed to dry and a 10µL drop of supernatant from each strain culture filtered using 0.22uM filter was spotted on each overlay. After an additional drying step, the plates were incubated overnight at 37°C and the production of colicin was identified by the presence of an inhibition halo when the filtered supernatant was spotted. LB was spotted as a negative control and filtered supernatant from both strains was also spotted on overlay of each of them to be sur that the growth inhibition halo was not due to the presence of Mitomycin C in the filtered supernatant.

Whole genome sequencing and analysis

Prior to genome extraction, a single colony of each strain was inoculated in LB medium for over-day culture till the OD_{600} reached around 1.0 (ca. $5.0x10^8$ bacteria/mL). The bacterial cells were collected from 2mL of the culture and the genomic DNA was extracted using the Wizard Genomic DNA Purification Kit (Promega). Samples were then sent to Novogene Co., Ltd to be sequenced using Illumina NovaSeq 6000. Sequencing reads were pre-processed to remove low-quality or artefactual bases. We used fqCleaner v.0.5.0, a mini workflow implemented in Galaxy [8] (https://galaxy.pasteur.fr/) to process fastq files (quality trimming, duplicate and artifact filters). Draft genomes were de novo assembled using SPAdes version 3.15.0 [9] and annotated using Proka version 1.14.5 [10]. Assembly quality and completeness was assessed using BUSCO version v5.4.2 [11]. The assembled genomes were used for in silico typing and characterization of each strain using tools available at the Centre of Genomic Epidemiology (http://www.genomicepidemiology.org/): Resfinder [12–14], MLST [14,15], SerotypeFinder [16], CHtyper [17]. Phylogroups were identified in silico using ClermonTyping tool [18]. In order to identify contigs corresponding to potential plasmids, each contig was used as a query in a BLASTn search using blast+ version 2.2.31 [14] against the COMPASS database [19]. Only hits with 95% identity and 80% coverage of both the query and the hit sequence were kept.

Alternative strategy for competition assays of I2 vs R2 strains

Even if we managed to introduce GFP and RFP (mars) tags in I2 and R2 strains, the related proteins were likely not expressed since thefluorescence was impossible to detect. Consequently we used an alternative strategy to assess the proportion of each strain. We took andvantage of the fact that both strains can be differentiated by SNPs. An aliquot of the mixed culture containing 10^7 cells was pelleted and resuspended in 50µL of sterile distiled water and boiled for 10 minutes. Specific primers were then used to amplify a SNP locus in butC gene

and Sanger sequence the resulting DNA fragment. Then, using QSVanalyzer [20], we calculated the frequeny of each mutation and used it to compute the relative fitness as above.

To assess the accuracy of this strategy, we used strains I1 and R1 taged with different fluorescent marker to compare strains proportions as assessed by FACS and QSVanalyzer and found a very good correspondance between both methods (Supplemenatry Figure S6), therefore validating our alternative approach.

Western blot analysis and LPS gel

The heat extracted proteins from 1mL at OD_{600}=1 culture were suspended in 1×Laemmli buffer and incubated for 5 min at 95°C. The protein extracts were run on Mini-PROTEAN TGX Stain-Free precast Gels (BioRad) in 1×TGX buffer and then transferred to nitrocellulose membrane using a Trans-Blot® Turbo Transfer System (BioRad). Blocking was performed in a 5% solution of dry milk and 0.05% Tween 1×PBS (1×PBST) overnight at 4°C with agitation. The membranes were then incubated in 1×PBST with either rabbit anti-flagellin (kindly given by Dr Monica Rolando) or mouse anti-RNAPα (BioLegend #663104) diluted 1/5,000 for 1h at room temperature with agitation. Membranes were washed in 1×PBST and then incubated with the secondary antibody (anti-rabbit or anti-mouse IgG conjugated with horse radish peroxidase at 1:10 000, Promega). The membranes were then revealed using an ECL kit (GE Healthcare) and the iBright™ CL1500 system (Thermofisher).

LPS analysis on Mini-PROTEAN TGX Stain-Free precast Gels (BioRad) were realized as in [21].

References

1. Sprouffske K, Wagner A. Growthcurver: an R package for obtaining interpretable metrics from microbial growth curves. BMC Bioinformatics. **2016**; 17(1):172.
2. Luria SE, Delbrück M. Mutations of Bacteria from Virus Sensitivity to Virus Resistance. Genetics. **1943**; 28(6):491–511.
3. Hall BM, Ma C-X, Liang P, Singh KK. Fluctuation AnaLysis CalculatOR: a web tool for the determination of mutation rate using Luria–Delbrück fluctuation analysis. Bioinformatics. **2009**; 25(12):1564–1565.
4. Phan QT, Sipka T, Gonzalez C, Levraud J-P, Lutfalla G, Nguyen-Chi M. Neutrophils use superoxide to control bacterial infection at a distance. PLOS Pathog. Public Library of Science; **2018**; 14(7):e1007157.
5. Renshaw SA, Loynes CA, Trushell DMI, Elworthy S, Ingham PW, Whyte MKB. A transgenic zebrafish model of neutrophilic inflammation. Blood. **2006**; 108(13):3976–3978.
6. Boucontet L, Passoni G, Thiry V, et al. A Model of Superinfection of Virus-Infected Zebrafish Larvae: Increased Susceptibility to Bacteria Associated With Neutrophil Death. Front Immunol. **2018**; 9:1084.
7. Mostowy S, Boucontet L, Mazon Moya MJ, et al. The zebrafish as a new model for the in vivo study of Shigella flexneri interaction with phagocytes and bacterial autophagy. PLoS Pathog. **2013**; 9(9):e1003588.
8. Mareuil F, Doppelt-Azeroual O, Ménager H. A public Galaxy platform at Pasteur used as an execution engine for web services . F1000Research [Internet]. **2017** [cited 2023 Feb 7]; 6. Available from: https://f1000research.com/posters/6-1030
9. Bankevich A, Nurk S, Antipov D, et al. SPAdes: a new genome assembly algorithm and its applications to single-cell sequencing. J Comput Biol J Comput Mol Cell Biol. **2012**; 19(5):455–477.
10. Seemann T. Prokka: rapid prokaryotic genome annotation. Bioinforma Oxf Engl. **2014**; 30(14):2068–2069.
11. Simão FA, Waterhouse RM, Ioannidis P, Kriventseva EV, Zdobnov EM. BUSCO: assessing genome assembly and annotation completeness with single-copy orthologs. Bioinforma Oxf Engl. **2015**; 31(19):3210–3212.
12. Bortolaia V, Kaas RS, Ruppe E, et al. ResFinder 4.0 for predictions of phenotypes from genotypes. J Antimicrob Chemother. **2020**; 75(12):3491–3500.
13. Zankari E, Allesøe R, Joensen KG, Cavaco LM, Lund O, Aarestrup FM. PointFinder: a novel web tool for WGS-based detection of antimicrobial resistance associated with chromosomal point mutations in bacterial pathogens. J Antimicrob Chemother. **2017**; 72(10):2764–2768.
14. Camacho C, Coulouris G, Avagyan V, et al. BLAST+: architecture and applications. BMC Bioinformatics. **2009**; 10:421.
15. Larsen MV, Cosentino S, Rasmussen S, et al. Multilocus sequence typing of total-genome-sequenced bacteria. J Clin Microbiol. **2012**; 50(4):1355–1361.
16. Joensen KG, Tetzschner AMM, Iguchi A, Aarestrup FM, Scheutz F. Rapid and Easy In Silico Serotyping of Escherichia coli Isolates by Use of Whole-Genome Sequencing Data. J Clin Microbiol. **2015**; 53(8):2410–2426.
17. L R, Tb J, F H, et al. CHTyper, a Web Tool for Subtyping of Extraintestinal Pathogenic Escherichia coli Based on the fumC and fimH Alleles. J Clin Microbiol [Internet]. J Clin Microbiol; **2018** [cited 2023 Feb 22]; 56(4). Available from:

https://pubmed.ncbi.nlm.nih.gov/29436420/
18. Beghain J, Bridier-Nahmias A, Le Nagard H, Denamur E, Clermont O. ClermonTyping: an easy-to-use and accurate in silico method for Escherichia genus strain phylotyping. Microb Genomics. **2018**; 4(7):e000192.
19. Douarre P-E, Mallet L, Radomski N, Felten A, Mistou M-Y. Analysis of COMPASS, a New Comprehensive Plasmid Database Revealed Prevalence of Multireplicon and Extensive Diversity of IncF Plasmids. Front Microbiol. **2020**; 11:483.
20. Carr IM, Robinson JI, Dimitriou R, Markham AF, Morgan AW, Bonthron DT. Inferring relative proportions of DNA variants from sequencing electropherograms. Bioinforma Oxf Engl. **2009**; 25(24):3244–3250.
21. Szczesny M, Beloin C, Ghigo J-M. Increased Osmolarity in Biofilm Triggers RcsB-Dependent Lipid A Palmitoylation in Escherichia coli. mBio. **2018**; 9(4):e01415-18.